J. Plasma Phys. (2025), *vol*. 91, E108
doi:10.1017/S0022377825100585

Spatio-temporal evolution and phase mixing of dust acoustic waves in plasmas with opposite polarity dust grains

Anubhab Biswas[1] **and Chandan Maity**[1]

[1]Department of Physics, Jadavpur University, Kolkata 700 032, India

Corresponding author: Chandan Maity, chandan.maity1986@gmail.com

(Received 28 March 2025; revision received 9 June 2025; accepted 9 June 2025)

A theoretical investigation on the space–time evolution of low-frequency dust acoustic waves (DAWs) in opposite polarity dusty plasmas reveals that they undergo phase mixing for arbitrary initial amplitudes, causing them to suffer a gradual loss in coherency. Both positively and negatively charged dynamical dust grains have been considered to coexist in the plasma, in addition to Maxwell–Boltzmann distributed hot electrons and ions. A perturbative analysis of the governing fluid-Maxwell equations leads us to conclude that the competing dynamics of the opposite polarity dust grains is what causes the DAWs to phase mix. An estimate for the phase-mixing time has also been obtained, which has been found to be profoundly influenced by the values of the various plasma parameters, such as the equilibrium densities of the plasma species, the masses of the opposite polarity dust grains and the electron and ion temperatures. The investigation has also been extended to include phase mixing of DAWs in electron-depleted dusty plasmas. The findings of this study are expected to have relevance in various astrophysical and laboratory plasma environments.

Key words: plasma waves, plasma nonlinear phenomena, dusty plasmas

1. Introduction

The study of dusty plasmas has been a cornerstone of research in plasma physics for the past few decades. Such an enormous interest in this regard can primarily be attributed to the fact that these plasmas are ubiquitous in various cosmic as well as terrestrial environments, such as in the planetary ring systems, in the Jovian magnetosphere, in cometary tails, in supernova remnants, in the Earth's polar mesosphere, in the Earth's magnetosphere, etc. (Goertz 1989; Havnes *et al*. 1996; Verheest 2000; Wahlund *et al*. 2009; Shukla & Mamun 2010; Morooka *et al*. 2011). They have also been extensively investigated in numerous laboratory environments (Barkan, Merlino & D'Angelo 1995; Merlino *et al*. 1998; Nakamura & Bailung 1999; Merlino *et al*. 2012*b*). Dusty plasmas differ significantly from other multicomponent plasmas and they are often far more complex than the usual plasmas in terms of the physics involved. It is the presence of massive charged dust grains in addition to the usual

electrons, ions and neutral atoms, in the plasma medium that is responsible for the increased complexity, as it leads to new collective phenomena on completely different space and time scales. Another layer of complexity arises from the consideration of the physical processes that lead to the charging of the dust grains (Whipple, Northrop & Mendis 1985; Shukla & Mamun 2010). The most widely used dusty plasma models assume the dust grains to be negatively charged. Such an assumption is justified given that the major method by which the dust grains essentially acquire charge is through the capture of background plasma particles (*viz.* electrons and ions), and since electrons are much more mobile than ions, the massive dust grains tend to capture more electrons and become negatively charged. Nevertheless, other important charging mechanisms have been identified that lead to positively charged dust grains, for e.g. secondary electron emission from the dust grain surface (Chow, Mendis & Rosenberg 1994), ultraviolet photon flux-induced photoemission (Rosenberg & Mendis 1995), thermionic emission due to radiative heating (Rosenberg, Mendis & Sheehan 1999), etc.

There is also direct evidence for the existence of dusty plasmas containing both positively and negatively charged dust grains, in addition to the usual plasma particles. Such plasmas are called opposite polarity dusty plasmas, and they have been found in different space environments, such as cometary tails, the Earth's polar mesosphere, etc. (Mendis & Rosenberg 1994; Horányi 1996; Havnes *et al*. 1996). The existence of opposite polarity dusty plasmas has been theorised quite a while ago. Meyer-Vernet (1982) reported that different charging histories could lead dust grains with similar electrical properties, present in the same plasma, to acquire opposite polarities. Chow, Mendis & Rosenberg (1993) theoretically showed that the size of the dust grains influences the process of secondary electron emission from the grain surface, and as such concluded that insulating dust grains with different sizes can acquire different polarities, the larger grains being negative while the smaller ones are positive. However, the opposite case, where the larger dust grains acquire a positive charge and the smaller ones negative, is also possible by means of triboelectric charging (Shukla & Rosenberg 2006). This has been predicted on the basis of observations in the Martian environment (Farrell *et al*. 2004) as well as in laboratory devices (Zhao *et al*. 2002, 2003). Thus, arguably, the most important property of opposite polarity dusty plasmas is that the ratio of the size of the negative to the size of the positive dust grains can be smaller or greater or even equal to unity.

Like any other plasma medium, dusty plasmas are also capable of supporting a number of waves, with the two most notable ones being the dust acoustic waves (DAWs) and the dust ion acoustic waves. Rao, Shukla & Yu (1990) first theoretically predicted the existence of DAWs in plasmas containing electrons, ions and negatively charged dust grains. Dust acoustic waves are very low-frequency waves and are characterised by a phase velocity that is much smaller than the electron and ion thermal speeds. For dust acoustic oscillations, the dust grains are considered to be inertial, as they provide the necessary inertia for the oscillation. On the other hand, the electron and ion thermal pressures are responsible for providing the requisite restoring force. The dust grains, being much more massive than the electrons and ions, have a comparatively higher oscillation period. Thus, during dust dynamics, there is ample time for the electrons and ions to balance out the electric force with the pressure gradient, and hence become inertialess in the process. As a result, the electrons and ions are described using the Maxwell–Boltzmann (MB) distribution. Ever since their prediction, DAWs in dusty plasmas with either single or opposite polarity dust grains have been at the forefront of research in plasma

https://doi.org/10.1017/S0022377825100585 Published online by Cambridge University Press

physics, and there exists numerous studies on them, both theoretical (Verheest *et al*. 1997; Rao 1998; Sakanaka & Shukla 2000; Shukla 2000; D'Angelo 2001; Shukla 2001; Rosenberg 2002; Singh 2002; Shukla 2003; Verheest, Hellberg & Kourakis 2008; Verheest 2009; Mamun & Shukla 2011; Mamun & Mannan 2011; Merlino *et al*. 2012*a*; El-Taibany 2013; Merlino 2014; Chakrabarti & Ghosh 2015) and experimental (Barkan *et al*. 1995; D'Angelo & Merlino, 1996; Rosenberg & Kalman 1997; Merlino *et al*. 1998; Bandyopadhyay *et al*. 2008; Merlino 2009; Merlino *et al*. 2012*b*; Deka *et al*. 2017). Here, we should mention that an important and plausible situation for opposite polarity dusty plasmas is the almost complete depletion of electrons, on account of them being captured by the dust grains during the charging process. This gives rise to what is known as electron-depleted dusty plasmas. Such plasmas are widely encountered in various space observations (Goertz 1989; Mendis & Rosenberg 1994; Morooka *et al*. 2011) as well as in laboratory environments (Goertz, Greiner & Piel 2011; Petersen *et al*. 2022). The properties of nonlinear DAWs in electron-depleted dusty plasmas has also been extensively studied (Tribeche & Merriche 2011; Mamun, Ferdousi & Sultana 2015; Tadsen *et al*. 2015; Shikha *et al*. 2019).

It is a known fact that plasmas cannot sustain waves of arbitrarily large amplitudes. Rather, for every plasma there exists a characteristic threshold value of wave steepness beyond which it can no longer sustain the wave. In fact, the moment the steepness of the wave goes beyond the threshold value, the wave no longer remains coherent, and this is indicated by the multivalued nature of the resultant waveform. This is termed as wave breaking (Dawson 1959; Davidson 1972) and it has been extensively studied over the years (Coffey 1971; Katsouleas & Mori 1988; Maity *et al*. 2013; Maity & Karmakar 2023; Biswas & Maity 2024*b*). The phenomenon has also been well investigated for DAWs (Heinrich, Kim & Merlino 2009; Shukla & I 2010; Flanagan & Goree 2011; Heinrich *et al*. 2012; Trukhachev *et al*. 2019). The cause for the steepening and the subsequent breaking of the high amplitude self-excited DAWs in these studies has been attributed to the generation of secondary harmonics, which arise inadvertently due to the inherent nonlinearity of the system. In this paper, we report that DAWs in opposite polarity dusty plasmas can also undergo wave breaking via a novel process, called phase mixing.

Phase mixing is a process through which excited waves/oscillations in plasmas lose their coherence and break even when their amplitude is well below the threshold value (Sen Gupta & Kaw 1999). Thus, phase mixing causes the waves to break at arbitrary amplitudes. It is a physical process which comes into effect on account of the characteristic frequency of the relevant plasma mode acquiring a spatial dependence. This causes the plasma species at different locations to oscillate with their respective local frequencies, which in turn leads to a secular increase in the phase difference between the neighbouring oscillators with time. Ultimately, a moment arrives when their trajectories overlap, causing the waves to lose their coherence and break. Over the years, extensive studies on phase mixing of a host of different waves and oscillations have been performed. This has allowed us to identify multiple physical processes and scenarios, such as finite ion inertia (Sen Gupta & Kaw 1999), inhomogeneity in the background ion density (Infeld, Rowlands & Torvén 1989), relativistic mass variation of electrons (Drake *et al*. 1976; Infeld & Rowlands 1989; Xu, Sheng & Zhang 2006; Maity *et al*. 2013; Pramanik & Maity 2021), inhomogeneous magnetic field (Maity, Chakrabarti & Sengupta 2012), multi-species dynamics (Verma 2011; Maity 2014; Pramanik, Maity & Chakrabarti 2015; Pramanik & Maity 2017, 2018; Maity & Pramanik 2020; Biswas & Maity 2024*a*; Pramanik, Biswas &

https://doi.org/10.1017/S0022377825100585 Published online by Cambridge University Press

Maity 2024; Biswas, Maity & Pramanik 2025), etc. which have been identified as the underlying cause for phase mixing. A number of numerical and experimental studies (Xu *et al*. 2006; Sengupta *et al*. 2009; Yu *et al*. 2016; Sahai 2017) have verified the validity of the phase-mixing process.

When an excited wave in a plasma breaks, the electrostatic wave energy associated with it is irreversibly converted into random particle motion. This causes the plasma medium to heat up, and as such phase mixing plays an important role in the field of plasma heating (Hasegawa & Chen 1974; Koch & Albritton 1974). Another area where phase mixing has an important application is in the field of plasma-based particle accelerators (Joshi *et al*. 1984; Modena *et al*. 1995; Malka 2012). When an electron beam or an intense laser is directed through a plasma medium, it leads to the generation of wake waves through charge separation. The strong electric field associated with the wake waves is then responsible for accelerating charged particles. This mechanism allows us to accelerate charged particles up to energies of the order of giga-electron volts over very small distances. This acceleration process is profoundly influenced by the phase-mixing process. If the phase-mixing time is shorter than the 'dephasing time', it can prevent the charged particles from acquiring maximum energy within the 'dephasing length'.

In this paper, we use the one-dimensional fluid-Maxwell equations to model the opposite polarity dusty plasmas, and employ a straightforward perturbation scheme (Nayfeh 2000; Holmes 2013) to study the explicit space–time evolution of the excited DAWs. The perturbative scheme used has been demonstrated to be capable of effectively capturing the essential aspects of the phase-mixing process, a key one being the appearance of secular terms in the analytical expressions for the fluid-field variables (Sen Gupta & Kaw 1999). We expect the results of our study to have relevance in various astrophysical scenarios, such as Saturn's magnetosphere (Kopnin, Shokhrin & Popel 2022), the Martian atmosphere (Izvekova, Reznichenko & Popel 2020), etc., as well as laboratory environments, such as fusion devices (De Angelis 2006), where the existence of DAWs has been well established. We also believe that the present study might lead to a better understanding of collective nonlinear phenomena in dusty plasmas.

The layout of the paper is as follows: in § 2 we have presented the basic fluid-Maxwell equations governing the dynamics of the DAWs in opposite polarity dusty plasmas. We have presented the relevant linear dispersion relation as well. Section 3 contains the nonlinear analysis of the basic equations using a simple perturbative expansion method, which demonstrates the phase mixing of the excited DAWs. The section also contains an approximate expression for the phase-mixing time. In § 4, a detailed discussion on how the phase-mixing time is affected by the plasma parameters is presented. Finally, we summarise our results and draw appropriate conclusions in § 5.

2. Basic equations and linear dispersion relation

We consider a four-component collisionless, homogeneous and unmagnetised dusty plasma consisting of cold positively and negatively charged dust grains, hot singly ionised isothermal ions and hot isothermal electrons. The quasineutrality condition for the plasma is given as $n_{+0} + n_{i0} = n_{-0} + n_{e0}$, where n_{+0} (n_{-0}), n_{i0} and n_{e0} are the equilibrium densities of the positive (negative) dust grains, the ions and electrons, respectively. We have defined $n_{+0} = Z_+ N_{+0}$ ($n_{-0} = Z_- N_{-0}$), where $Z_+ > 0$ ($Z_- > 0$) and N_{+0} (N_{-0}) denote the constant amount of charge and equilibrium number densities of the positive (negative) dust grains, respectively. Here, we

https://doi.org/10.1017/S0022377825100585 Published online by Cambridge University Press

have neglected the dust charge fluctuations due to varying electron and ion currents to the dust particles. Our analysis involves the utilisation of the one-dimensional fluid model along the x-direction. For low-frequency DAWs, the hot ions and electrons are considered to be inertialess fluids, and as such their densities (n_i and n_e, respectively) are given by the MB-distribution, as follows:

$$n_i = n_{i0} \exp\left(-\frac{e\phi}{T_i}\right), \tag{2.1}$$

$$n_e = n_{e0} \exp\left(\frac{e\phi}{T_e}\right). \tag{2.2}$$

Here, e is the electronic charge, ϕ is the electrostatic wave potential and T_i (T_e) is the temperature of the ions (electrons) in energy units. Note that the ion temperature is always less than the electron temperature, i.e. $T_i < T_e$.

The cold dust grains (both positive and negative), on the other hand, take part in the wave dynamics and as a result have been considered inertial. The continuity and momentum equations govern the dynamics of the charged dust grains which are, respectively,

$$\partial_t n_\pm + \partial_x (n_\pm v_\pm) = 0, \quad \text{and} \tag{2.3}$$

$$\partial_t v_\pm + v_\pm \partial_x v_\pm = \pm \frac{Z_\pm e}{m_\pm} E, \tag{2.4}$$

for positively charged dust grains (+) and negatively charged dust grains (−). Here, $n_\pm$, $v_\pm$ and $m_\pm$ denote the densities, the x-component of the fluid velocities and masses of the two types of charged dust grains in the plasma. Note that, in accordance with our previous definition, the dust densities are given as $n_+ = Z_+ N_+$ for the positively charged grains, and as $n_- = Z_- N_-$ for the negatively charged grains, with N_+ and N_- denoting the respective number densities. Also, E represents the $x-$component of the electric field, and is related to the electrostatic wave potential ϕ as $E = -\partial_x \phi$. Finally, to close the system of equations, namely (2.3) and (2.4), we use the Poisson's equation as

$$\partial_x E = -\partial_x^2 \phi = 4\pi e(n_i + n_+ - n_e - n_-). \tag{2.5}$$

A straightforward linearisation of (2.1) to (2.5) yields the following dispersion relation:

$$1 + \frac{1}{k^2 \lambda_D^2} = \frac{\omega_+^2 + \omega_-^2}{\omega^2}, \tag{2.6}$$

where $\omega_+ = \sqrt{4\pi N_{+0} Z_+^2 e^2 / m_+}$ is the dust plasma frequency of the positively charged dust grains, $\omega_- = \sqrt{4\pi N_{-0} Z_-^2 e^2 / m_-}$ is the dust plasma frequency of the negatively charged dust grains and $1/\lambda_D^2 = 1/\lambda_{Di}^2 + 1/\lambda_{De}^2$ with $\lambda_{Di} = \sqrt{T_i / 4\pi e^2 n_{i0}}$ being the ion Debye length and $\lambda_{De} = \sqrt{T_e / 4\pi e^2 n_{e0}}$ being the electron Debye length. In addition to this, ω and k represent the frequency and wavenumber of the excited DAWs, respectively. In the long wavelength limit ($k^2 \lambda_D^2 \ll 1$) we can rewrite the above dispersion relation as

$$\omega = k C_{DA} \sqrt{1 + Z\eta\mu}, \tag{2.7}$$

https://doi.org/10.1017/S0022377825100585 Published online by Cambridge University Press

where $C_{DA} = Z_-^{1/2}(n_{-0}/n_{i0})^{1/2}(T_i/m_-)^{1/2}[1+(n_{e0}T_i/n_{i0}T_e)]^{-1/2}$ is the dust acoustic speed, $Z = Z_+/Z_-$, $\eta = n_{+0}/n_{-0}$ and $\mu = m_-/m_+$. The factor $Z\eta\mu$ in (2.7) appears as a consequence of considering two different kinds of dynamical dust grains (positively and negatively charged), and accordingly it vanishes if either $\eta \to 0$ (or, $n_{+0} \to 0$), implying that there are no positively charged dust grains, or if $\mu \to 0$ (or, $m_+ \to \infty$), implying that positively charged dust grains are present, but are static. In § 3, we will illustrate that when a nonlinear analysis of the problem is performed, it is the presence of this factor which yields interesting effects for the DAWs in plasmas with opposite polarity dust grains, one of them being phase mixing. Note that, in the absence of the positively charged dust grains, the dispersion relation given by (2.6) or (2.7) immediately reduces to the form as reported in Rao *et al*. (1990) and Shukla & Mamun (2010).

3. Nonlinear analysis

3.1. *Perturbation method and first-order solutions*

Before commencing with the perturbative analysis, we first introduce the following new normalised variables, with the objective of simplifying the subsequent calculations

$$\begin{aligned} &\Delta n_s = \Delta n_+ + \Delta n_-, \quad \Delta n_d = \Delta n_+ - \Delta n_-, \\ &\Delta v_s = v_+ + v_- \quad \text{and} \quad \Delta v_d = v_+ - v_-, \end{aligned} \tag{3.1}$$

where $\Delta n_+ = n_+ - \eta$ and $\Delta n_- = n_- - 1$. Thus, the basic (2.3) to (2.5) can be rewritten in terms of these new variables as

$$\partial_t(\Delta n_d) + \frac{1}{2}\partial_x[(\eta+1)\Delta v_d + (\eta-1)\Delta v_s + \Delta n_s \Delta v_d + \Delta n_d \Delta v_s] = 0, \tag{3.2a}$$

$$\partial_t(\Delta n_s) + \frac{1}{2}\partial_x[(\eta+1)\Delta v_s + (\eta-1)\Delta v_d + \Delta n_s \Delta v_s + \Delta n_d \Delta v_d] = 0, \tag{3.2b}$$

$$\partial_t(\Delta v_s) + \frac{1}{4}\partial_x(\Delta v_s^2 + \Delta v_d^2) = -(1 - Z\mu)E, \tag{3.2c}$$

$$\partial_t(\Delta v_d) + \frac{1}{2}\partial_x(\Delta v_s \Delta v_d) = (1 + Z\mu)E, \tag{3.2d}$$

$$\partial_x E = \Delta n_d - \delta_i\left[1 - \exp\left(-\frac{\sigma\phi}{T}\right)\right] + \delta_e\left[1 - \exp\left(\frac{\phi}{T}\right)\right]. \tag{3.2e}$$

Here, we have utilised the respective normalised expressions for the densities of the hot MB-distributed ions and electrons which are

$$n_i = \delta_i \exp\left(-\frac{\sigma\phi}{T}\right), \tag{3.3}$$

$$n_e = \delta_e \exp\left(\frac{\phi}{T}\right). \tag{3.4}$$

The normalisations for all the variables involved in (3.2*a*) to (3.2*e*), and (3.3) and (3.4) have been presented in table 1. Also, we have defined $\sigma = T_e/T_i$, $T = Z_- T_e k^2/m_-\omega^2$, $\delta_i = n_{i0}/n_{-0}$ and $\delta_e = n_{e0}/n_{-0}$, such that $\eta = 1 + \delta_e - \delta_i$ in accordance with the quasineutrality condition.

https://doi.org/10.1017/S0022377825100585 Published online by Cambridge University Press

Variables	Normalised by	Normalised variables
Space	k^{-1}	x
Time	ω_-^{-1}	t
Densities	n_{-0}	n_+, n_-, n_i, n_e
Dust fluid velocities	$\omega_- k^{-1}$	v_+, v_-
Electric field	$m_-\omega_-^2 Z_-^{-1} e^{-1} k^{-1}$	E
Electrostatic potential	$m_-\omega_-^2 Z_-^{-1} e^{-1} k^{-2}$	ϕ

TABLE 1. Normalisation scheme.

The spatio-temporal evolution of the excited DAWs is investigated by employing a simple perturbative expansion method where all the fluid-field variables $\psi(x,t)$ are expanded as $\psi(x,t) = \sum_{j=0}^{\infty} \psi^{(j)}(x,t)$ (Nayfeh 2000; Holmes 2013). Here, the jth expansion term $\psi^{(j)}$ is proportional to the jth power of a small expansion parameter ϵ. We then insert this expansion into (3.2*a*) to (3.2*e*) and solve for successive orders of the perturbations in the fluid-field variables, subject to the following initial conditions:

$$\Delta n_d(x,0) = -(1 + Z\eta\mu)\,\epsilon \cos x, \tag{3.5a}$$

$$\Delta n_s(x,0) = (1 - Z\eta\mu)\,\epsilon \cos x, \tag{3.5b}$$

$$\Delta v_d(x,0) = \Delta v_s(x,0) = 0. \tag{3.5c}$$

Here, the small expansion parameter ϵ serves as the perturbation amplitude. In terms of the original unnormalised variables, these initial conditions are

$$n_-(x,0) = n_{-0}(1 + \epsilon \cos kx), \tag{3.6a}$$

$$n_+(x,0) = n_{+0}(1 - Z\mu\epsilon \cos kx), \tag{3.6b}$$

$$v_+(x,0) = v_-(x,0) = 0. \tag{3.6c}$$

Note that, when we expand $\exp(\phi/T)$ and $\exp(-\sigma\phi/T)$, we retain only the linear terms and ignore all the higher-order ones. In other words, we expand them as $1 + (\phi/T)$ and $1 - (\sigma\phi/T)$, respectively. This is justified as $e\phi \ll T_i, T_e$ for DAWs.

On substituting the perturbative expansions of the fluid-field variables into (3.2*a*) to (3.2*e*), and collecting terms that are proportional to ϵ, yields the following first-order equations for all the variables involved:

$$\partial_t(\Delta n_d^{(1)}) + \frac{1}{2}\partial_x[(\eta+1)\Delta v_d^{(1)} + (\eta-1)\Delta v_s^{(1)}] = 0, \tag{3.7a}$$

$$\partial_t(\Delta n_s^{(1)}) + \frac{1}{2}\partial_x[(\eta+1)\Delta v_s^{(1)} + (\eta-1)\Delta v_d^{(1)}] = 0, \tag{3.7b}$$

$$\partial_t(\Delta v_s^{(1)}) = -(1 - Z\mu)E^{(1)}, \tag{3.7c}$$

https://doi.org/10.1017/S0022377825100585 Published online by Cambridge University Press

$$\partial_t(\Delta v_d^{(1)}) = (1 + Z\mu)E^{(1)}, \tag{3.7d}$$

$$\partial_x E^{(1)} = \Delta n_d^{(1)} - \left(\frac{\sigma\delta_i + \delta_e}{T}\right)\phi^{(1)}. \tag{3.7e}$$

In keeping with our goal of investigating the spatio-temporal evolution of DAWs, we aim to construct solutions to (3.7*a*) to (3.7*e*) that are separable, i.e. solutions that can be written as products of two functions, one which has an explicit dependence on x, while the other has an explicit dependence on t (standing wave solutions). Since, the initial (first-order) perturbation has been taken to be proportional to $\epsilon \cos x$, we can write $\partial_x E^{(1)} = -\partial_x^2\phi^{(1)} = \phi^{(1)}$, which allows us to write the following expression for ϕ:

$$\phi^{(1)} = \gamma_1 \Delta n_d^{(1)}, \tag{3.8}$$

with $\gamma_1 = (1 + (\sigma\delta_i + \delta_e)/T)^{-1}$. On using (3.7*a*) to (3.7*e*) along with (3.8), we obtain the following homogeneous differential equation for $\Delta n_d^{(1)}$

$$\partial_t^2(\Delta n_d^{(1)}) + \Omega^2 \Delta n_d^{(1)} = 0, \tag{3.9}$$

where $\Omega = \sqrt{\gamma_1(1 + Z\eta\mu)}$. Finally, on utilising the initial conditions given by (3.5*a*) to (3.5*c*), we arrive at the following expressions for the first-order perturbations in the fluid-field variables (first-order solutions):

$$\Delta n_d^{(1)} = -\epsilon a_1 \cos x \cos \Omega t, \tag{3.10a}$$

$$\Delta n_s^{(1)} = \epsilon a_2 \cos x \cos \Omega t, \tag{3.10b}$$

$$\Delta v_d^{(1)} = -\epsilon b_1 \sin x \sin \Omega t, \tag{3.10c}$$

$$\Delta v_s^{(1)} = \epsilon b_2 \sin x \sin \Omega t, \tag{3.10d}$$

$$\phi^{(1)} = -\epsilon\gamma_1 a_1 \cos x \cos \Omega t, \tag{3.10e}$$

$$E^{(1)} = -\epsilon\gamma_1 a_1 \sin x \cos \Omega t, \tag{3.10f}$$

where we have defined $a_1 = 1 + Z\eta\mu$, $a_2 = 1 - Z\eta\mu$, $b_1 = \Omega(1 + Z\mu)$ and $b_2 = \Omega(1 - Z\mu)$. As expected, the first-order solutions, given by (3.10*a*) to (3.10*f*), are purely standing wave solutions, obtained as the superposition of two travelling waves propagating in opposite directions. Expectedly, as of now the first-order equations show no indication of phase mixing, meaning we must extend our analysis to the second-order perturbations in the fluid-field variables.

3.2. *Second-order solutions*

Proceeding in a similar fashion as in § 3.1, we can construct the equations for the second-order perturbations in the fluid-field variables by substituting the perturbative expansions of the variables into (3.2*a*) to (3.2*e*), and collecting terms that are proportional to ϵ^2. Just as before, we aim for solutions that are separable, i.e. standing

https://doi.org/10.1017/S0022377825100585 Published online by Cambridge University Press

wave solutions. Owing to the convective nonlinearity of the plasma medium, the perturbations in the second-order analysis will be proportional to $\epsilon^2 \cos 2x$. As a result, this allows us to write $\partial_x E^{(2)} = -\partial_x^2 \phi^{(2)} = 4\phi^{(2)}$. Thus, we have

$$\phi^{(2)} = \frac{\gamma_2}{4} \Delta n_d^{(2)}, \tag{3.11}$$

where $\gamma_2 = (1 + (\sigma\delta_i + \delta_e)/4T)^{-1}$. Using the second-order equations so constructed along with (3.11), we obtain the following non-homogeneous differential equation for $\Delta n_d^{(2)}$:

$$\partial_t^2(\Delta n_d^{(2)}) + \Omega_1^2 \Delta n_d^{(2)} = \frac{1}{4}(\eta + 1)\, \partial_x^2 \left[\Delta v_s^{(1)} \Delta v_d^{(1)}\right] + \frac{1}{8}(\eta - 1)\, \partial_x^2 \left[\Delta v_s^{(1)^2} + \Delta v_d^{(1)^2}\right] - \frac{1}{2}\partial_x \partial_t \left[\Delta n_s^{(1)} \Delta v_d^{(1)} + \Delta n_d^{(1)} \Delta v_s^{(1)}\right], \tag{3.12}$$

where $\Omega_1 = \sqrt{\gamma_2(1 + Z\eta\mu)}$. On utilising the proper initial conditions, $\Delta n_d^{(2)}(x, 0) = 0$ and $\partial_t \Delta n_d^{(2)}(x, 0) = 0$, we end up with the following expression for $\Delta n_d^{(2)}$:

$$\Delta n_d^{(2)} = \epsilon^2 \cos 2x \left[\frac{d_0}{\Omega_1^2}(1 - \cos \Omega_1 t) + \frac{d_1}{\Omega_1^2 - 4\Omega^2}(\cos 2\Omega t - \cos \Omega_1 t)\right]. \tag{3.13}$$

Once we have $\Delta n_d^{(2)}$, it is straightforward to obtain the relevant expressions for the second-order perturbations in the remaining fluid-field variables (second-order solutions) from the second-order equations. These remaining second-order solutions turn out to be as follows:

$$\phi^{(2)} = \frac{1}{2}\epsilon^2 \cos 2x\, (e_0 + e_1 \cos \Omega_1 t + e_2 \cos 2\Omega t), \tag{3.14a}$$

$$E^{(2)} = \epsilon^2 \sin 2x\, (e_0 + e_1 \cos \Omega_1 t + e_2 \cos 2\Omega t), \tag{3.14b}$$

$$\Delta v_s^{(2)} = -\epsilon^2 \sin 2x\, (g_0 t + g_1 \sin \Omega_1 t + g_2 \sin 2\Omega t), \tag{3.14c}$$

$$\Delta v_d^{(2)} = \epsilon^2 \sin 2x\, (h_0 t + h_1 \sin \Omega_1 t + h_2 \sin 2\Omega t), \tag{3.14d}$$

$$\Delta n_s^{(2)} = \epsilon^2 \cos 2x\, [\alpha t^2 + c_1(1 - \cos \Omega_1 t) + c_2(1 - \cos 2\Omega t)]. \tag{3.14e}$$

The expressions for all the coefficients in the second-order solutions are presented below

$$d_0 = -\frac{(\eta + 1)b_1 b_2}{4} + \frac{(\eta - 1)(b_1^2 + b_2^2)}{8},$$

$$d_1 = \frac{(a_1 b_2 + a_2 b_1)\Omega}{2} + \frac{(\eta + 1)b_1 b_2}{4} - \frac{(\eta - 1)(b_1^2 + b_2^2)}{8}.$$

$$e_0 = \frac{d_0 \gamma_2}{2\Omega_1^2}, \quad e_1 = -\frac{d_0 \gamma_2}{2\Omega_1^2} - \frac{d_1 \gamma_2}{2(\Omega_1^2 - 4\Omega^2)}, \quad e_2 = \frac{d_1 \gamma_2}{2(\Omega_1^2 - 4\Omega^2)},$$

$$g_0 = e_0(1 - Z\mu) + \frac{1}{8}(b_1^2 + b_2^2), \quad g_1 = \frac{e_1}{\Omega_1}(1 - Z\mu),$$

$$g_2 = \frac{1}{2\Omega}\left[e_2(1 - Z\mu) - \frac{1}{8}(b_1^2 + b_2^2)\right],$$

https://doi.org/10.1017/S0022377825100585 Published online by Cambridge University Press

$$h_0 = e_0(1+Z\mu) + \frac{1}{4}(b_1 b_2),\ \ h_1 = \frac{e_1}{\Omega_1}(1+Z\mu),\ \ h_2 = \frac{1}{2\Omega}\left[e_2(1+Z\mu) - \frac{1}{4}(b_1 b_2)\right],$$
$$\alpha = \frac{1}{2}[(\eta+1)g_0 - (\eta-1)h_0],\ \ c_1 = \frac{1}{\Omega_1}[(\eta+1)g_1 - (\eta-1)h_1],$$
$$c_2 = \frac{1}{2\Omega}\left[(\eta+1)g_2 - (\eta-1)h_2 - \left(\frac{a_1 b_1 + a_2 b_2}{4}\right)\right]. \tag{3.15}$$

The second-order solutions clearly depict that, during the evolution of the excited DAWs, higher harmonics in both space and time are generated. This is a direct consequence of the inherent nonlinearity of the plasma medium. In addition to this, we also see that there now exists a new mode of oscillation with frequency Ω_1. This new mode arises due to the presence of the MB-distributed hot ions and electrons whose number densities are always dependent on ϕ, i.e. $n_{i,e} \equiv n_{i,e}(\phi)$. Another important feature of the second-order solutions is the presence of direct current (DC) and secular terms, the DC terms being those that have no dependence on t, while the secular terms are those that are proportional to t or t^2, and as such have an unbounded growth with evolving time. It must be stressed here that the presence of such secular terms, which are driven by terms like $\sim \partial_x^2\left(\Delta v_s^{(1)^2} + \Delta v_s^{(1)^2}\right)$ and $\sim \partial_x^2\left(\Delta v_s^{(1)}\Delta v_s^{(1)}\right)$ in the second-order equations, are in no way an artefact of the perturbation method employed. Rather, such secular terms serve as important signatures of phase mixing (Sen Gupta & Kaw 1999). Consider the secular term $\sim (\epsilon^2\alpha\cos 2x)t^2$ in the expression for $\Delta n_s^{(2)}$. Physically, such a secular term is indicative of rapid bunching of plasma particles in space with time. Here, the constant α is given as

$$\alpha = \frac{1}{2}[(\eta+1)g_0 - (\eta-1)h_0], \tag{3.16}$$

which, on using the expressions for g_0 and h_0 and simplifying appropriately, can be rewritten as

$$\alpha = \frac{Z\eta\mu\gamma_1}{2}(1+Z\mu). \tag{3.17}$$

Thus, we notice that the presence and the subsequent effects of the secular term in $\Delta n_s^{(2)}$ on the evolution of DAWs in opposite polarity dusty plasmas is determined solely by the values of the plasma parameters η and μ. In the limit $\eta \to 0$, which implies the absence of positively charged dust grains, we end up with $\alpha \to 0$. This indicates that there would be no secular terms in the second-order solutions in the presence of only single polarity dust grains. Alternatively, in the limit $\mu \to 0$, implying that the positively charged dust grains are stationary, we again end up with $\alpha \to 0$. Thus, in order to ensure the appearance of secular terms in the second-order solutions, it is not only necessary to have both positive and negative polarity dust grains, but also necessary to consider them both to be dynamical.

On examining the expression for $E^{(2)}$ (and $\phi^{(2)}$ as well), we notice the presence of a DC term, which signifies the existence of a non-zero ponderomotive force. This becomes evident when one averages the electric field over the oscillation time scale. The plasma particles respond to this non-zero ponderomotive force and undergo a spatial rearrangement, thereby rendering the plasma medium inhomogeneous. In such an inhomogeneous medium, the characteristic frequency of the relevant mode acquires a spatial dependence, and is no longer constant. What happens is that, as the DAWs self-consistently evolve in space and time, the plasma particles start to

https://doi.org/10.1017/S0022377825100585 Published online by Cambridge University Press

accumulate at certain locations while moving away from others, giving rise to spikes in the density profile. This is embodied by the presence of the secular term in $\Delta n_s^{(2)}$. Thus, the excited DAWs eventually lose their coherency, and are said to be phase mixed.

3.3. *Estimating the phase-mixing time*

To obtain an estimate of the phase-mixing time, we first construct an approximate evolution equation for Δn_d correct up to third order as

$$\partial_t^2 \Delta n_d + \Omega^2 \left[1 + \frac{1+Z\mu}{2(1+Z\eta\mu)} \Delta n_s\right] \Delta n_d \approx 0. \tag{3.18}$$

On substituting the leading-order secular term for Δn_s, which is $\Delta n_s^{(2)} \approx (\epsilon^2 \alpha \cos 2x) t^2$, (3.18) transforms to

$$\partial_t^2 \Delta n_d + \Omega^2 (1 + \mathcal{B} t^2 \cos 2x) \Delta n_d \approx 0, \tag{3.19}$$

where

$$\mathcal{B} = \frac{\epsilon^2 \alpha}{2} \left(\frac{1+Z\mu}{1+Z\eta\mu}\right).$$

Using the initial conditions $\Delta n_d(x, 0) = -a_1 \epsilon \cos x$ and $\partial_t \Delta n_d(x, 0) = 0$, we write the following Wentzel–Kramers–Brillouin (WKB) solution (Bender & Orszag 2009) for (3.19):

$$\Delta n_d \approx -a_1 \epsilon \cos x \cos\left[\Omega t \left(1 + \frac{\mathcal{B} t^2}{6} \cos 2x\right)\right]. \tag{3.20}$$

Notice that, in accordance with our earlier discussion, the characteristic frequency of the dust acoustic mode has indeed acquired a spatial dependence, in addition to a dependence on η and μ. This is what leads to the phase mixing of the excited DAWs.

The initial perturbation to the plasma at $t = 0$ excites the primary mode of the DAWs. As time progresses, higher harmonics are generated. This happens at the expense of the electrostatic energy that was initially loaded into the primary mode, wherein it cascades irreversibly to the higher harmonics with evolving time. As a result, the primary mode suffers an eventual collisionless decay. This becomes evident when we expand (3.20) in terms of a Bessel series (Watson 2006) as follows:

$$\begin{aligned}\Delta n_d \approx -\frac{1}{2} a_1 \epsilon \sum_{l=-\infty}^{+\infty} J_l\left(\frac{1}{6}\mathcal{B}\Omega t^3\right) \Bigg[\cos\left(\Omega t + \frac{l\pi}{2}\right) \{\cos(2l+1)x + \cos(2l-1)x\} \\ + \sin\left(\Omega t + \frac{l\pi}{2}\right) \{\sin(2l+1)x + \sin(2l-1)x\}\Bigg].\end{aligned} \tag{3.21}$$

(3.21) shows that the amplitude of the primary mode ($l = 0$) varies as $\sim J_0(\mathcal{B}\Omega t^3/6)$, which clearly indicates the decay of the primary mode as time progresses. Additionally, (3.21) depicts the subsequent generation of higher harmonics ($l = 1, 2, \ldots$) as well. Finally, on using $J_0(\mathcal{B}\Omega t^3/6) \approx J_0(1)$, we obtain an approximate expression for the phase-mixing time $\omega_- t_{mix}$ as

$$\omega_- t_{mix} = \frac{1}{\sqrt{\gamma_1}} \left[\frac{24\sqrt{1+Z\eta\mu}}{\epsilon^2 Z\eta\mu(1+Z\mu)^2}\right]^{1/3}. \tag{3.22}$$

https://doi.org/10.1017/S0022377825100585 Published online by Cambridge University Press

Note that, when $\eta \to 0$ (implying that there are no positive dust grains), the phase-mixing time becomes infinitely high, i.e. $\omega_- t_{mix} \to \infty$. This is also the case when the limit $\mu \to 0$ (implying that the positive dust grains are at rest) is considered. Thus, in keeping with the discussion in § 3.2, we note that, for the excited DAWs to phase mix, the presence of both positively and negatively charged dynamical dust grains in the plasma is crucial.

Here, we must point out an apparent asymmetry in the applicability of (3.22) in determining the phase-mixing time of DAWs in plasmas with single polarity dust grains. Up until now, the utilisation of proper limits has allowed us to successfully apply (3.22) to predict the phase-mixing time for DAWs in plasmas containing only negatively charged dynamical dust grains, which is found to be infinitely high. But it turns out that (3.22) cannot be used to do the same for DAWs in plasmas with only positively charged dust grains. To put it somewhat crudely, in the present analysis it is possible to switch off the positively charged dust grains (density and dynamics), but not the negatively charged ones. In other words, one cannot obtain the phase-mixing time for DAWs in plasmas with just positively charged dynamical dust grains from (3.22), by simply utilising the limits $\eta \to \infty$ and/or $\mu \to \infty$. Evidently, this is due to the fact that, for such limits, the phase-mixing time becomes zero ($\omega_- t_{mix} \to 0$), which bears no physical meaning. The reason behind this apparent asymmetry lies in the fact that the initial conditions chosen for the above analysis, given by (3.5*a*) to (3.5*c*) or (3.6*a*) to (3.6*c*), do not support such an operation and in the limits $\eta \to \infty$ and $\mu \to \infty$, the initial conditions become meaningless. One must bear in mind that the situation where only the negatively charged dynamical dust grains are present is completely different from the one where it is just the positively charged dynamical dust grains. This is made evident by the stark contrast in the quasineutrality relation and the basic equations for the two cases.

In order to be able to switch off the negatively charged dust grains and obtain the correct estimate for the phase-mixing time in plasmas with positively charged dynamical dust grains, we must consider an alternative set of initial conditions. This would yield a different expression for the phase-mixing time in comparison with (3.22), which would allow us to switch off the negatively charged dust grains by utilising the appropriate limiting conditions. But, this new set of initial conditions would also suffer from the same asymmetry as it would no longer allow us to switch off the positively charged dust grains. However, the final conclusion, i.e. that excited DAWs in dusty plasmas undergo phase mixing only if the plasma contains both positively and negatively charged dynamical dust grains, would remain unaltered.

3.4. *Phase-mixing time of DAWs in electron-depleted dusty plasmas*

A plausible scenario for a dusty plasma with opposite polarity dust grains is one where, during the charging of the dust grains, almost all the electrons have attached themselves onto the surface of the grains. Thus, the resulting plasma is almost entirely depleted of electrons, and now consists of just three major components, the positively charged dust grains, the negatively charged dust grains and the hot isothermal ions. Note that the keyword here is almost, since a complete depletion of the electrons is not possible. This is due to the fact that the minimum value for the ratio of the electron to ion equilibrium number density is given by the square root of the ratio of the electron to ion mass, when the electron and ion temperatures are approximately equal and the grain surface potential is zero (Shukla & Mamun 2010;

https://doi.org/10.1017/S0022377825100585 Published online by Cambridge University Press

Tribeche & Merriche 2011). Thus, for electron-depleted dusty plasmas we have

$$\frac{n_{e0}}{n_{i0}} = \sqrt{\frac{m_e}{m_i}}, \tag{3.23}$$

where m_e (m_i) denotes the mass of the electrons (ions). If we consider the ions to be that of hydrogen (H^+), then the electron to ion mass ratio has the value $m_e/m_i = 1/1836$. On using (2.1) and (2.2), and normalising the electron and ion densities in (3.23) appropriately (see table 1), we obtain the minimum value of δ_e in an electron-depleted dusty plasma as

$$\delta_e \approx 0.023\delta_i, \tag{3.24}$$

which leads to the following quasineutrality condition:

$$\eta + 0.977\delta_i = 1. \tag{3.25}$$

As it turns out, such electron-depleted plasmas can still support DAWs, and accordingly, the linear dispersion relation is found to be

$$1 + \frac{1.023}{k^2\lambda_{Di}^2} = \frac{\omega_+^2 + \omega_-^2}{\omega^2}, \tag{3.26}$$

which in the long wavelength limit can be written as

$$\omega = kC_{DA}\sqrt{1 + Z\eta\mu}. \tag{3.27}$$

Here, $C_{DA} = 0.9887Z_-^{1/2}(n_{-0}/n_{i0})^{1/2}(T_i/m_-)^{1/2}$ is the dust acoustic speed. These DAWs will also undergo phase mixing, with the estimate for the phase-mixing time being given as

$$\omega_- t_{mix} = \sqrt{1 + \frac{\delta_i}{\beta_i}}\left[\frac{24\sqrt{1 + Z\eta\mu}}{\epsilon^2 Z\eta\mu(1 + Z\mu)^2}\right]^{1/3}, \tag{3.28}$$

where $\beta_i = Z_- k^2 T_i/1.023 m_- \omega_-^2$ is a constant. The above estimate for the phase-mixing time has been directly obtained from (3.22), after having modified the expression for γ_1 as $\gamma_1 = (1 + \delta_i/\beta_i)^{-1}$.

4. Parametric analysis of the phase-mixing time

In this section, we investigate how the phase-mixing time of DAWs in the usual opposite polarity dusty plasmas as well as in electron-depleted dusty plasmas, is affected by variations in the values of the different plasma parameters η, μ and σ. In order to proceed with the parametric analysis, we choose certain typical values for the various plasma quantities (Barkan *et al*. 1995; D'Angelo & Merlino 1996; D'Angelo 2001; Shukla & Mamun 2010; Mamun & Shukla 2011). These are presented in table 2. In the discussions that follow, the values for the plasma parameters that have been utilised are in conjunction with the values in table 2. For instance, if we use $\sigma = 100$ in our discussions, then this would immediately provide us with the value for T_e as 2.5 eV, since we have chosen T_i to be equal to 0.025 eV.

https://doi.org/10.1017/S0022377825100585 Published online by Cambridge University Press

Plasma quantity	Value
Z_-	10^3
Z_+	10
T_i	0.025 eV
N_{-0}	10^4 cm^{-3}
m_-	2.3×10^{-15} g
k	1 cm^{-1}

TABLE 2. Typical values for the plasma quantities.

In the usual opposite polarity dusty plasmas, on utilising the values in table 2 and setting $\eta = 1.2$, $\delta_i = 0.2$, $\sigma = 50$ and $\mu = 100$, which implies that the negatively charged dust grains are heavier in comparison with the positively charged ones, the corresponding plasma frequencies for the positively and negatively charged dust grains turn out to be $\omega_+ = 3887$ and $\omega_- = 3548$ rad s^{-1}, respectively. This in turn yields 427.5 rad s^{-1} as the DAW frequency ω, which is approximately 68 Hertz. Similarly, on setting $\mu = 0.01$ instead, i.e. on considering the positively charged dust grains to be heavier than the negatively charged ones, the corresponding DAW frequency turns out to be approximately 46 Hertz. Thus, the frequency of DAWs in either case is quite low, which is expected (Shukla & Mamun 2010). Proceeding in a similar fashion, one can obtain a typical value for the DAW frequency in electron-depleted plasmas as well by utilising the values in table 2 and considering $\eta = 0.8$, $\delta_i = 0.2047$ and $\mu = 100$ or $\mu = 0.01$. The relevant DAW frequency then turns out to be approximately 61 Hertz when $\mu = 100$, and approximately 45.8 Hertz when $\mu = 0.01$, which is expectedly quite low again.

4.1. *Variation of the phase-mixing time with η*

In figure 1, we show the variation of the phase-mixing time with η for four different cases. Recall that η is the ratio of the equilibrium density of the positively charged dust grains to that of the negatively charged ones ($\eta = n_{+0}/n_{-0}$). Thus, an increasing value of η essentially signifies an increasing value of n_{+0} in comparison with n_{-0}. In figures 1(*a*) and 1(*b*), the variation in the phase-mixing time with η is shown, whilst keeping δ_i fixed at 0.2. Following from the quasineutrality condition, such a consideration immediately constrains the values that η can attain, as now we must have $\eta > 1 - \delta_i$ (which is $\eta > 0.8$ in our case), in order to ensure that δ_e always remains positive. Thus, we have considered the variation in η for the two plots to be in the range $0.805 \leqslant \eta \leqslant 25$. On the other hand, in figures 1(*c*) and 1(*d*), we have kept δ_e fixed at 0.4, and have allowed δ_i to be modified with changing η. This again imposes a constraint on the values that η can attain, which turns out to be $\eta < 1 + \delta_e$ (i.e. $\eta < 1.4$ in our case). Just as before, this constraint on η follows from the quasineutrality condition, and the fact that δ_i is always positive. Accordingly, the variation in η for the two plots in this case has been considered to lie in the range $0.05 \leqslant \eta \leqslant 1.39$. Additionally, the variations in figures 1(*a*) and 1(*b*) with fixed $\delta_i = 0.2$ is shown for two different values of μ, i.e. $\mu = 0.01$ and $\mu = 100$, respectively. This has also been done for figures 1(*c*) and 1(*d*) with fixed $\delta_e = 0.4$. The consideration of two different values for μ has been made in order

https://doi.org/10.1017/S0022377825100585 Published online by Cambridge University Press

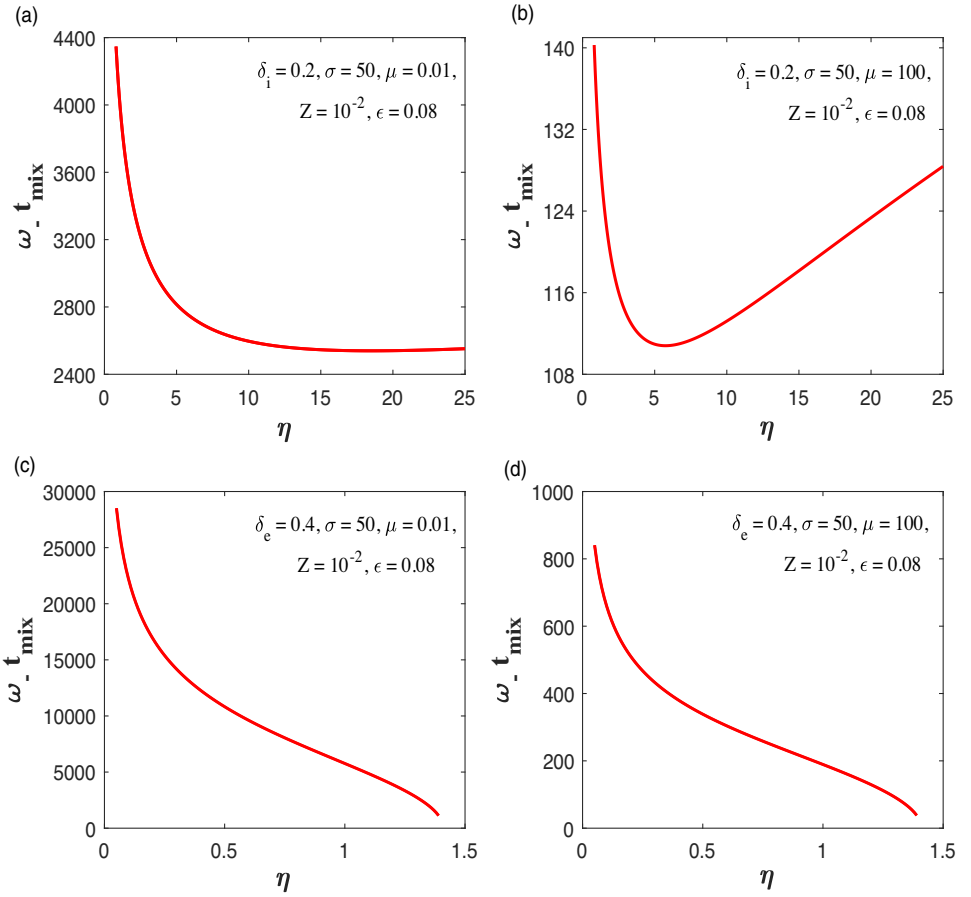

FIGURE 1. Variation of phase-mixing time ($\omega_{-}t_{mix}$) with η ($=n_{+0}/n_{-0}$) for (a) $\delta_i = 0.2$, $\sigma = 50$ and $\mu = 0.01$, (b) $\delta_i = 0.2$, $\sigma = 50$ and $\mu = 100$, (c) $\delta_e = 0.4$, $\sigma = 50$ and $\mu = 0.01$ and (d) $\delta_e = 0.4$, $\sigma = 50$ and $\mu = 100$. Here, $Z = 10^{-2}$ and $\epsilon = 0.08$.

to take into account the fact that dust grains with either polarity can be heavier than the other. Lastly, we have considered $\sigma = 50$, $Z = 10^{-2}$ and $\epsilon = 0.08$, as well.

Our primary observation is that, in figures 1(a) and 1(b), for small values of η the phase-mixing time is quite high, and as η increases, the phase-mixing time gradually decreases. But this decrease happens only up to a certain value of η, i.e. for $\eta = \eta_c$, and on increasing the value of η beyond η_c, the phase-mixing time starts to increase. In other words, for $\eta = \eta_c$, the phase-mixing time exhibits a minimum. In stark contrast to this, the variations in figures 1(c) and 1(d) depict that, with increasing η, the initially high phase-mixing time decreases gradually, but exhibits no minimum. The reason behind such distinctly different variations in the two sets of plots lies in the fact that the quasineutrality condition for the plasma is profoundly influenced by whether we allow δ_e or δ_i to be modified with increasing η, whilst keeping the other fixed. This becomes evident when we consider the expression for the phase-mixing time for the two cases. If we keep δ_i fixed then the quasineutrality condition dictates that, with increasing η, δ_e increases as well. The expression for the phase-mixing

https://doi.org/10.1017/S0022377825100585 Published online by Cambridge University Press

time, given by (3.22), is then modified as

$$\omega_{-}t_{mix} = \left[\frac{24\sqrt{1+Z\eta\mu}}{\epsilon^2 Z\eta\mu(1+Z\mu)^2}\left(\alpha_i + \frac{\eta}{T}\right)^{3/2}\right]^{1/3}, \tag{4.1}$$

where $\alpha_i = 1 + (\delta_i(\sigma+1) - 1)/T$. On the other hand, if we keep δ_e fixed, the quasineutrality condition dictates that, with increasing η, δ_i decreases and the expression for the phase-mixing time is then modified as

$$\omega_{-}t_{mix} = \left[\frac{24\sqrt{1+Z\eta\mu}}{\epsilon^2 Z\eta\mu(1+Z\mu)^2}\left(\alpha_e - \frac{\sigma\eta}{T}\right)^{3/2}\right]^{1/3}, \tag{4.2}$$

where, $\alpha_e = 1 + (\delta_e(\sigma+1) + \sigma)/T$. Thus, (4.1) and (4.2) clearly show how the choice of considering either δ_i or δ_e to be fixed leads to vastly different quasineutrality situations for the plasma, which in turn affects the phase-mixing time of DAWs.

The secondary observation that we make is that a higher value of μ leads to lower overall values for the phase-mixing time. This is true irrespective of whether we keep δ_i or δ_e fixed, as seen from figures 1(*a*) to 1(*d*). A detailed discussion on this is presented in § 4.2. Note that, for the variation with fixed δ_i in figures 1(*a*) and 1(*b*), we find that the value of μ also affects the value of η_c. Indeed, this becomes evident when one writes the expression for η_c as follows:

$$\eta_c = \frac{Z\mu\alpha_i T - 1 + \sqrt{1 + Z^2\mu^2\alpha_i^2 T^2 + 14Z\mu\alpha_i T}}{4Z\mu}. \tag{4.3}$$

Accordingly, for $\mu = 0.01$, we have $\eta_c = 18.49$ in figure 1(*a*), while for $\mu = 100$, we have $\eta_c = 5.75$ in figure 1(*b*). Note that (4.3) shows us that η_c is also dependent on σ, and as such, the variation of η_c with μ and σ is presented in figures 2(*a*) and 2(*b*), respectively. In figure 2(*a*), the variation in μ has been taken to lie in the range $0.01 \leqslant \mu \leqslant 100$, and we can clearly see that, with increasing μ, η_c decreases continuously. On the other hand, figure 2(*b*) shows us that on increasing the value of σ in the range $10 \leqslant \sigma \leqslant 200$, the value of η_c increases, almost linearly. Thus, the increasing values of the parameters μ and σ have completely opposite effects on the value of η_c, i.e. the former causes it to decrease monotonically while the latter causes it to increase monotonically.

In figure 3, we have again shown the variation of the phase-mixing time as a function of η, but for two different values of σ, which are (1) $\sigma = 50$ (denoted as the red solid line) and (2) $\sigma = 150$ (denoted as the blue dashed line). Just as before, we have considered the two different cases of either keeping δ_i fixed at 0.2 (see figure 3*a*), or keeping δ_e fixed at 0.4 (see figure 3*b*), whilst allowing the other parameter to change with changing η. As expected, in figure 3(*a*), the phase-mixing time exhibits a minimum. Note that, for smaller values of η, the two curves corresponding to the two different σ values are almost merged as one. In reality, however, the phase-mixing time for $\sigma = 150$ is lower than that for $\sigma = 50$, but the difference is quite small in comparison with the overall variation with η. As η increases, we notice that the two curves start to deviate from one another, and as η is increased further, the phase-mixing time gradually approaches its minimum value at $\eta = \eta_c$, Here, we notice that, for the higher value of $\sigma = 150$, the value for the minimum phase-mixing time is much lower in comparison with that for $\sigma = 50$.

https://doi.org/10.1017/S0022377825100585 Published online by Cambridge University Press

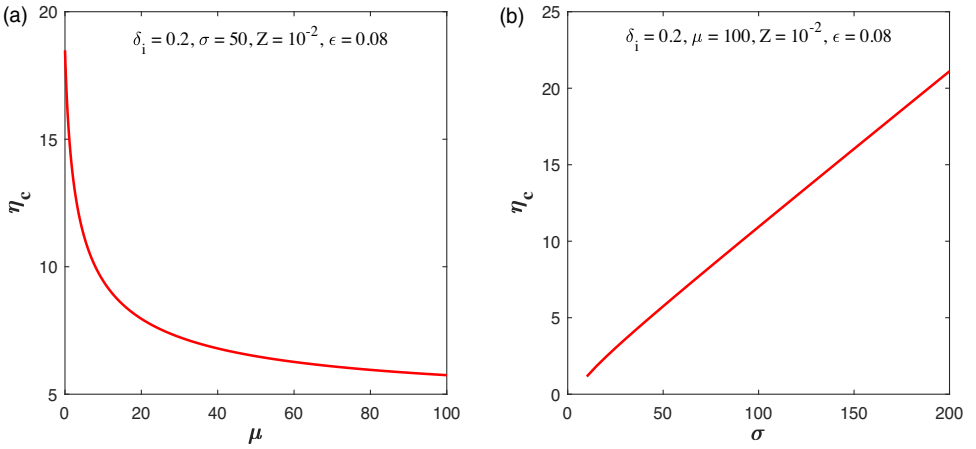

FIGURE 2. Variation of η_c with (*a*) μ for $\sigma = 50$, and (*b*) σ for $\mu = 10$. Here, $\delta_i = 0.2$, $Z = 10^{-2}$ and $\epsilon = 0.08$.

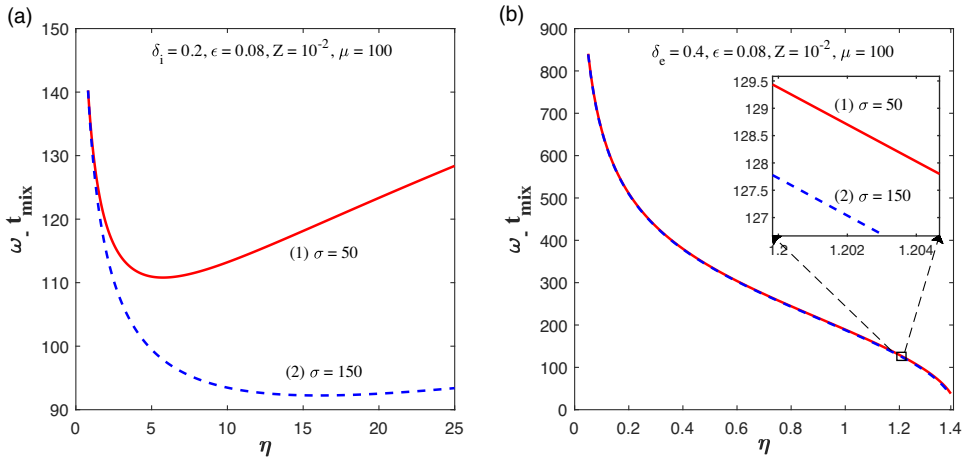

FIGURE 3. Variation of phase-mixing time ($\omega_- t_{mix}$) with $\eta\ (= n_{+0}/n_{-0})$ for (*a*) δ_i kept fixed at 0.2, and (*b*) δ_e kept fixed at 0.4. The variation in both (*a*) and (*b*) is shown for two distinct values of σ, (1) $\sigma = 50$ (red solid curve) and (2) $\sigma = 150$ (blue dashed curve). In panel (*b*) a zoomed in version of the original plot around $\eta = 1.202$ is embedded, in order to clearly bring forth the effect of σ on the phase-mixing time. Also, we have considered $\mu = 10$, $Z = 10^{-2}$ and $\epsilon = 0.08$.

In figure 3(*b*), as δ_e has been kept fixed, we observe no minimum for the phase-mixing time. Here, we see that the two curves, (1) and (2), corresponding to two different values of $\sigma = 50$ and $\sigma = 150$, respectively, are completely merged as one. What has happened is that the overall variation in the phase-mixing time with η is so large in comparison with the variation in it for two different σ, that the two curves seem to have merged into a single one. In order to alleviate any confusion regarding this and to confirm that different values of σ do indeed affect the phase-mixing time even in this case, we have embedded in the figure 3(*b*) a zoomed in version

https://doi.org/10.1017/S0022377825100585 Published online by Cambridge University Press

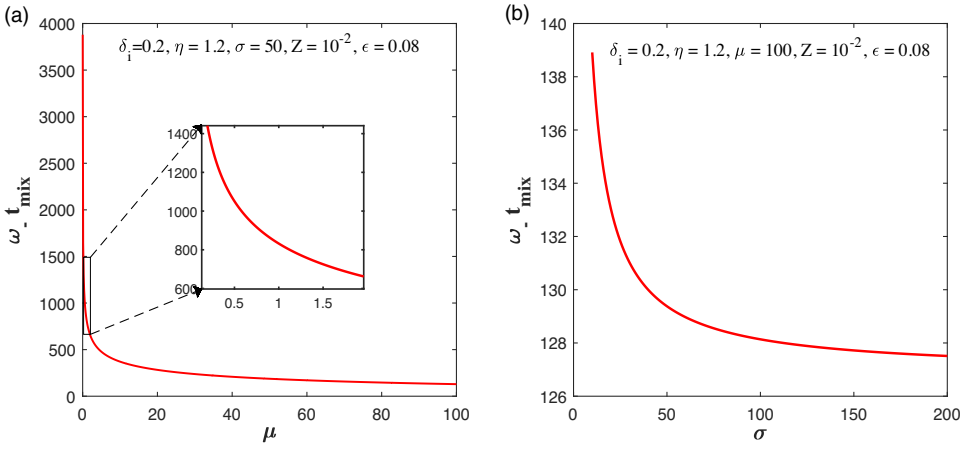

FIGURE 4. Variation of phase-mixing time ($\omega_- t_{mix}$) with (*a*) μ ($= m_-/m_+$) for $\sigma = 50$, and (*b*) σ for $\mu = 100$. Here, we have considered $\delta_i = 0.2$, $\eta = 1.2$, $Z = 10^{-2}$, and $\epsilon = 0.08$.

of the original plot at around $\eta = 1.202$. This clearly shows that, just as before, a higher value of σ leads to a lower phase-mixing time. We discuss the variation of the phase-mixing time with σ in greater detail in § 4.2.

4.2. *Variation of the phase-mixing time with μ and σ*

In this section we conduct a detailed parametric analysis of the variation of the phase-mixing time with μ and σ. Recall that μ is defined as the ratio of the mass of the negatively charged dust grains to that of the positively charged ones (i.e. $\mu = m_-/m_+$), while σ is defined as the ratio of the temperature of the MB-distributed electrons to that of the MB-distributed ions (i.e. $\sigma = T_e/T_i$). Thus, increasing values of μ and σ signify an increasing value of m_- and T_e, respectively, in comparison with m_+ and T_i, respectively.

The variation of the phase-mixing time with μ is depicted in figure 4(*a*) for $\delta_i = 0.2$, $\eta = 1.2$, $\sigma = 50$, $Z = 10^{-2}$ and $\epsilon = 0.08$. The range of values for μ has been chosen to be $0.01 \leqslant \mu \leqslant 100$, which ensures that the variation depicted as such takes into account the fact that it is possible for dust grains with either polarity to be heavier than the other, or they might even have equal masses. Figure 4(*a*) shows that the value of the phase-mixing time decreases very drastically for very small values of μ (i.e. for values corresponding to $m_+ \gg m_-$). This is represented by the almost vertical drop that the curve exhibits for values of μ that are very small. In order to bring out the variation in the phase-mixing time for such small values of μ, we have embedded a zoomed in version of the original plot in the figure. The zoomed in plot depicts the phase-mixing time at around $\mu = 1$. After the initial drastic fall in phase-mixing time, we observe that, as the value of μ increases, the phase-mixing time continues to decrease, albeit the rate at which it happens slows down considerably. Thus, higher values of μ cause the excited DAWs to phase mix quicker. This is in agreement with the secondary observation made from figure 1. Physically, what happens is that higher values of μ cause the overall initial perturbations in the fluid-field variables, given by (3.5*a*) to (3.5*c*), to become higher as well, even though the perturbation amplitude is kept constant at $\epsilon = 0.08$. This results in a quicker phase mixing of the excited DAWs.

https://doi.org/10.1017/S0022377825100585 Published online by Cambridge University Press

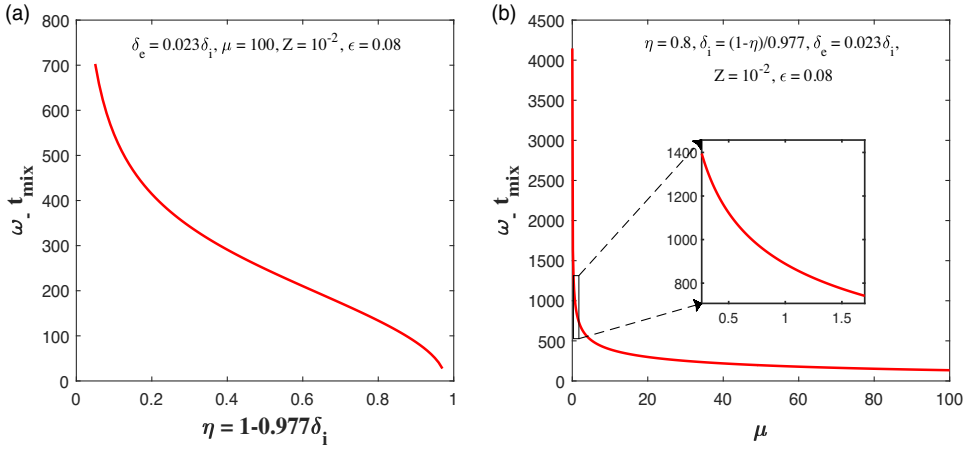

FIGURE 5. Variation of phase-mixing time ($\omega_- t_{mix}$) in an electron-depleted dusty plasma, with (*a*) η for $\mu = 100$, and (*b*) μ for $\eta = 0.8$. Additionally, here we have considered $\delta_e = 0.023\delta_i$, $Z = 10^{-2}$ and $\epsilon = 0.08$.

In figure 4(*b*) we have plotted the variation of the phase-mixing time with σ for $\delta_i = 0.2$, $\eta = 1.2$, $\mu = 100$, $Z = 10^{-2}$ and $\epsilon = 0.08$. Here, we have considered the variation in σ to lie in the range $10 \leqslant \sigma \leqslant 200$. Note that, since the electrons are much lighter than the ions, the electron temperature is always higher than the ion temperature. As such, we have $\sigma > 1$ always. From the figure, we see that, as σ increases, there is a monotonic decrease in the phase-mixing time, which immediately corroborates our observation from figure 3. The reason behind this is that a higher temperature for the electrons means a higher value of the electron thermal pressure, which in turn leads to a higher value of the electron pressure gradient force ($\sim T_e \partial_x P_e$). Thus, in order to maintain a MB-distribution for the electrons, a stronger electric field is required to nullify the higher value of the electron pressure gradient force. Such a stronger electric field leads the plasma medium to acquire a greater spatial inhomogeneity, which ultimately causes the excited DAWs to phase mix quicker.

4.3. *Variation of the phase-mixing time in electron-depleted dusty plasmas*

In § 3.4, we discussed the possibility of phase mixing of DAWs in electron-depleted dusty plasmas, and presented an expression for the phase-mixing time as well, given by (3.28). In this section we analyse how this phase-mixing time varies with parameters η, μ and β_i (or, equivalently T_i), which are characteristic to electron-depleted plasmas. Following the discussion in § 3.4, an electron-depleted dusty plasma cannot be completely depleted of electrons. Rather, there is a minimum value for the density of electrons in such plasmas. For our purposes, this value is considered to be $\delta_e = 0.023\delta_i$.

In figure 5(*a*), the variation of the phase-mixing time with η is depicted. Here, we have considered $\mu = 100$, $\beta_i = 1.35 \times 10^{-3}$ (which is equivalent to $T_i = 0.025$ eV), $Z = 10^{-2}$ and $\epsilon = 0.08$. Here, η lies in the range $0.05 \leqslant \eta \leqslant 0.99$, which is in accordance with the constraint $\eta < 1$. As this is an electron-depleted dusty plasma, meaning that the value of δ_e is fixed (at $0.023\delta_i$), the nature of the variation of the phase-mixing time is similar to the ones depicted in figures 1(*c*) and 1(*d*), i.e.

https://doi.org/10.1017/S0022377825100585 Published online by Cambridge University Press

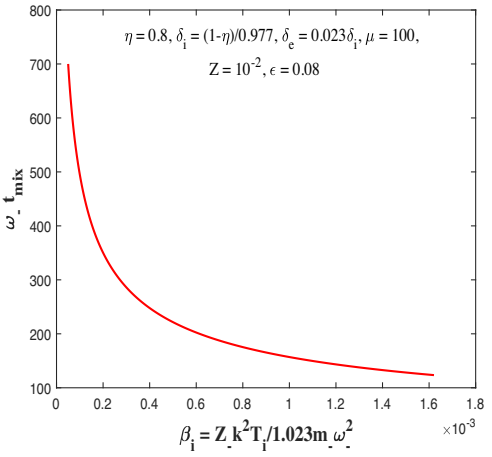

FIGURE 6. Variation of phase-mixing time (ω_t_{mix}) with β_i ($= Z\_k^2T_i/1.023m\_\omega_\_^2$) in an electron-depleted dusty plasma for $\eta = 0.8$, $\delta_i = (1-\eta)/0.977$, $\delta_e = 0.023\delta_i$, $\mu = 100$, $Z = 10^{-2}$ and $\epsilon = 0.08$.

with increasing η, the phase-mixing time decreases gradually, and exhibits no minimum. In figure 5(*b*), we have shown the variation of the phase-mixing time as a function of μ, where μ lies in the same range as before, which is $0.01 \leqslant \mu \leqslant 100$. In addition to this we have considered $\eta = 0.8$, $\delta_i = (1-\eta)/0.977 = 0.2047$, $\delta_e = 0.023\delta_i$, $\beta_i = 1.35 \times 10^{-3}$, $Z = 10^{-2}$ and $\epsilon = 0.08$. The variation in this case is almost entirely similar to that depicted in figure 4(*a*). For small values of μ the phase-mixing time is very high, and it drastically drops in value for slight increments in μ. Similar to figure 4(*a*), here too we have zoomed in at around $\mu = 1$, in order to clearly bring forth the change in the phase-mixing time with small values for μ. As μ keeps on increasing, the phase-mixing time continues to decrease, with the rate of decrement becoming smaller with higher values of μ. As discussed in § 4.2, the reason for such a variation can be realised from the fact that the value of μ greatly influences the initial perturbations to the fluid-field variables.

Figure 6 depicts the variation in the phase-mixing time of DAWs in electron-depleted dusty plasmas with β_i, which is defined as $\beta_i = Z\_k^2T_i/1.023m\_\omega_\_^2$. Note that increasing β_i essentially implies increasing values for the ion temperature T_i, and hence the variation in the phase-mixing time has in reality been analysed as a function of T_i. The variation in β_i in the figure has been considered to be in the range $0.0541 \times 10^{-3} \leqslant \beta_i \leqslant 1.62 \times 10^{-3}$, which is equivalent to $0.001\ \text{eV} \leqslant T_i \leqslant 0.03$ eV. Additionally, we have also considered $\eta = 0.8$, $\delta_i = (1-\eta)/0.977 = 0.2047$, $\delta_e = 0.023\delta_i$, $\mu = 100$, $Z = 10^{-2}$ and $\epsilon = 0.08$. As expected, we find that, for increasing values of β_i, the phase-mixing time decreases monotonically. This is also similar to the variation depicted in figure 4(*b*). Just as before, the reason behind such behaviour of the phase-mixing time with β_i is that, as β_i increases, or as T_i increases, the corresponding ion thermal pressure increases as well. This in turn leads to an increase in the pressure gradient force which then requires a higher electric field to balance it out, so as to maintain the MB-distribution for the ions. This increase in the electric field leads to an increase in the spatial inhomogeneity of the plasma, thereby ultimately reducing the phase-mixing time.

https://doi.org/10.1017/S0022377825100585 Published online by Cambridge University Press

In figures 1 to 6, the phase-mixing time has been scaled using the oscillation period of the negatively charged dust grains (ω_-^{-1}). In the usual opposite polarity dusty plasmas, on considering certain particular values for the plasma parameters, say for $\eta = 0.2$, $\delta_i = 0.2$, $\sigma = 50$ and $\mu = 100$, the phase-mixing time is found to be $\omega_- t_{mix} \approx 129$. In the actual time scale, this is equivalent to approximately 0.23 seconds. In terms of the period of the excited DAWs, the above phase-mixing time scales to $\omega t_{mix} \approx 16$. Similarly, in electron-depleted dusty plasmas, the phase-mixing time turns out to be $\omega_- t_{mix} \approx 144$, for $\eta = 0.8$, $\delta_i = 0.2047$, $\mu = 100$ and $\beta_i = 1.35 \times 10^{-3}$. Again, this is equivalent to approximately 0.26 seconds, and in terms of the DAW period it is $\omega t_{mix} \approx 15.67$.

5. Conclusion

We have studied the space–time evolution of DAWs in opposite polarity dusty plasmas, consisting of MB-distributed hot electrons and ions, and cold dynamical dust grains with opposite polarities. Our analysis, which involved using a simple perturbative treatment of the governing fluid-Maxwell equations, revealed that DAWs in such opposite polarity dusty plasmas undergo phase mixing, causing them to break at arbitrary amplitudes. We found that the competing dynamics of the two dust species was the sole reason behind the phase mixing of DAWs. As such, the coexistence of positively and negatively charged dynamical dust grains in the plasma medium is absolutely crucial for phase mixing of DAWs. The analysis has also been extended to include phase mixing of DAWs in electron-depleted dusty plasmas, where the density of the electrons was reduced to as low a value as theoretically possible. Our analytical findings illustrate that, as the DAWs evolve in space and time, a non-zero ponderomotive force is self-consistently generated, which causes the plasma medium to acquire a spatial inhomogeneity. This causes the characteristic mode frequency to become spatially dependent, which is what ultimately leads to phase mixing. An estimate for the phase-mixing time has also been presented for DAWs in both opposite polarity as well as electron-depleted dusty plasmas. One must bear in mind that the phase-mixing time of DAWs in certain limiting cases, such as in dusty plasmas with only positively charged dust grains, cannot be fruitfully extracted from the presented expression. This is due to the fact that the expression for the phase-mixing time obtained is specific to the initial conditions that we have used for our analysis. Utilisation of a different set of initial conditions is required for this purpose, but they too would turn out to be insufficient for some other limiting case. In other words, we have not been able to pinpoint any such set of initial conditions that would successfully incorporate all the limiting cases. The phase-mixing phenomenon for DAWs with certain alternative initial conditions will be addressed in future communications. Here, we must stress that, although the use of different initial conditions would lead to different expressions for the phase-mixing time, the final conclusion as to phase mixing of DAWs in opposite polarity dusty plasmas would remain identical to the one that we have obtained in our present study.

The present investigation also involves a detailed analysis of the effects that the various plasma parameters have on the phase-mixing time of DAWs, in both the usual opposite polarity dusty plasmas as well as in the electron-depleted dusty plasmas. We have found the phase-mixing time to be greatly influenced by the equilibrium densities of the plasma species, wherein it exhibits a minimum with increasing values of the ratio of the equilibrium dust density of the positively charged grains to that of

https://doi.org/10.1017/S0022377825100585 Published online by Cambridge University Press

the negatively charged ones. But this is true only if we allow the equilibrium density of the electrons to be modified with the increasing values of the ratio, whilst keeping the equilibrium ion density fixed. For the alternative case, however, no such minimum is observed. The phase-mixing time has also been noticed to be profoundly affected by the masses of the dynamical dust grains, such that it becomes very high if the positively charged ones are considered to be more massive than the negatively charged ones. Alternatively, if the opposite case is considered, then the phase-mixing time is found to be much lower. In addition to this, the temperature of the inertialess species has also been observed to considerably affect the phase-mixing time. Lastly, we would like to mention that studies have revealed that the electrons and ions in various space environments often obey certain distributions that deviate from the usual MB-distribution (Asbridge, Bame & Strong 1968; Lundin *et al*. 1989; Cairns *et al*. 1995; Futaana *et al*. 2003; Hellberg, Mace & Cattaert 2005), and as dusty plasmas capable of sustaining DAWs are ubiquitous in such environments, the present study can be extended to include such non-isothermal distributions for electrons and ions, and the dust charge fluctuations due to varying electron and ion currents. An investigation in this regard will be addressed in future publications. We believe that the results of our present investigation might bear relevance in space plasma as well as laboratory environments.

Acknowledgements

Editor Luís O. Silva thanks the referees for their advice in evaluating this article.

Declaration of interests

The authors report no conflict of interest.

REFERENCES

ASBRIDGE, J.R., BAME, S.J. & STRONG, I.B. 1968 Outward flow of protons from the Earth's bow shock. *J. Geophys. Res.* **73**, 5777–5782.

BANDYOPADHYAY, P., PRASAD, G., SEN, A. & KAW, P.K. 2008 Experimental study of nonlinear dust acoustic solitary waves in a dusty plasma. *Phys. Rev. Lett.* **101**, 065006.

BARKAN, A., MERLINO, R.L. & D'ANGELO, N. 1995 Laboratory observation of the dust-acoustic wave mode. *Phys. Plasmas* **2**, 3563–3565.

BENDER, C.M. & ORSZAG, S.A. 2009 *Advanced Mathematical Methods for Scientists and Engineers. 1: Asymptotic Methods and Perturbation Theory*. Springer.

BISWAS, A. & MAITY, C. 2024*a* Phase-mixing of high-frequency electrostatic oscillations in multicomponent dusty plasmas. *Pramana - J. Phys.* **98**, 51.

BISWAS, A. & MAITY, C. 2024*b* Wave-breaking limit of electrostatic waves in two-temperature electron-positron plasmas. *Phys. Scr.* **99**, 055601.

BISWAS, A., MAITY, C. & PRAMANIK, S. 2025 Phase-mixing of dust ion acoustic waves in plasmas. *Phys. Lett. A* **538**, 130355.

CAIRNS, R.A., MAMUM, A.A., BINGHAM, R., BOSTRÖM, R., DENDY, R.O., NAIRN, C.M.C. & SHUKLA, P.K. 1995 Electrostatic solitary structures in non-thermal plasmas. *Geophys. Res. Lett.* **22**, 2709–2712.

CHAKRABARTI, N. & GHOSH, S. 2015 Longitudinal dust acoustic solitary waves in a strongly coupled complex (dusty) plasma. *J. Plasma Phys.* **81**, 905810310.

CHOW, V., MENDIS, D. & ROSENBERG, M. 1994 Secondary emission from small dust grains at high electron energies. *IEEE Trans. Plasma Sci.* **22**, 179–186.

CHOW, V.W., MENDIS, D.A. & ROSENBERG, M. 1993 Role of grain size and particle velocity distribution in secondary electron emission in space plasmas. *J. Geophys. Res.* **98**, 19065–19076.

COFFEY, T.P. 1971 Breaking of large amplitude plasma oscillations. *Phys. Fluids* **14**, 1402–1406.
D'ANGELO, N. 2001 Dust-acoustic waves in plasmas with opposite polarity grains. *Planet. Space Sci.* **49**, 1251–1256.
D'ANGELO, N. & MERLINO, R. 1996 Current-driven dust-acoustic instability in a collisional plasma. *Planet. Space Sci.* **44**, 1593–1598.
DAVIDSON, R.C. 1972 Methods in nonlinear plasma theory. In *Pure and Applied Physics*, vol. 37, Academic Press.
DAWSON, J.M. 1959 Nonlinear electron oscillations in a cold plasma. *Phys. Rev.* **113**, 383–387.
DE ANGELIS, U. 2006 Dusty plasmas in fusion devices. *Phys. Plasmas* **13**, 012514.
DEKA, T., BORUAH, A., SHARMA, S.K. & BAILUNG, H. 2017 Observation of self-excited dust acoustic wave in dusty plasma with nanometer size dust grains. *Phys. Plasmas* **24**, 093706.
DRAKE, J.F., LEE, Y.C., NISHIKAWA, K. & TSINTSADZE, N.L. 1976 Breaking of large-amplitude waves as a result of relativistic electron-mass variation. *Phys. Rev. Lett.* **36**, 196–200.
EL-TAIBANY, W.F. 2013 Nonlinear dust acoustic waves in inhomogeneous four-component dusty plasma with opposite charge polarity dust grains. *Phys. Plasmas* **20**, 093701.
FARRELL, W.M., *et al.* 2004 Electric and magnetic signatures of dust devils from the 2000-2001 MATADOR desert tests. *J. Geophys. Res.* **109**, 2003JE002088.
FLANAGAN, T.M. & GOREE, J. 2011 Development of nonlinearity in a growing self-excited dust-density wave. *Phys. Plasmas* **18**, 013705.
FUTAANA, Y., MACHIDA, S., SAITO, Y., MATSUOKA, A. & HAYAKAWA, H. 2003 Moon-related non-thermal ions observed by Nozomi: species, sources, and generation mechanisms. *J. Geophys. Res.* **108**, 1025.
GOERTZ, C.K. 1989 Dusty plasmas in the solar system. *Rev. Geophys.* **27**, 271–292.
GOERTZ, I., GREINER, F. & PIEL, A. 2011 Effects of charge depletion in dusty plasmas. *Phys. Plasmas* **18**, 013703.
HASEGAWA, A. & CHEN, L. 1974 Plasma heating by Alfvén-wave phase mixing. *Phys. Rev. Lett.* **32**, 454–456.
HAVNES, O., TRØIM, J., BLIX, T., MORTENSEN, W., NAESHEIM, L.I., THRANE, E. & TØNNESEN, T. 1996 First detection of charged dust particles in the Earth's mesosphere. *J. Geophys. Res.* **101**, 10839–10847.
HEINRICH, J., KIM, S.-H. & MERLINO, R.L. 2009 Laboratory observations of self-excited dust acoustic shocks. *Phys. Rev. Lett.* **103**, 115002.
HEINRICH, J.R., KIM, S.-H., MEYER, J.K., MERLINO, R.L. & ROSENBERG, M. 2012 Secondary dust density waves excited by nonlinear dust acoustic waves. *Phys. Plasmas* **19**, 083702.
HELLBERG, M., MACE, R. & CATTAERT, T. 2005 Effects of superthermal particles on waves in magnetized space plasmas. *Space Sci. Rev.* **121**, 127–139.
HOLMES, M.H. 2013 Introduction to perturbation methods. In *Texts in Applied Mathematics*, vol. 20, Springer New York.
HORÁNYI, M. 1996 Charged dust dynamics in the solar system. *Annu. Rev. Astron. Astrophys.* **34**, 383–418.
INFELD, E. & ROWLANDS, G. 1989 Relativistic bursts. *Phys. Rev. Lett.* **62**, 1122–1125.
INFELD, E., ROWLANDS, G. & TORVÉN, S. 1989 Ion density cavities can cause nonlinear plasma oscillations to peak. *Phys. Rev. Lett.* **62**, 2269–2272.
IZVEKOVA, Y.N., REZNICHENKO, Y.S. & POPEL, S.I. 2020 On the possibility of dust acoustic perturbations in Martian ionosphere. *Plasma Phys. Rep.* **46**, 1205–1209.
JOSHI, C., MORI, W.B., KATSOULEAS, T., DAWSON, J.M., KINDEL, J.M. & FORSLUND, D.W. 1984 Ultrahigh gradient particle acceleration by intense laser-driven plasma density waves. *Nature* **311**, 525–529.
KATSOULEAS, T. & MORI, W.B. 1988 Wave-breaking amplitude of relativistic oscillations in a thermal plasma. *Phys. Rev. Lett.* **61**, 90–93.
KOCH, P. & ALBRITTON, J. 1974 Electron and ion heating through resonant plasma oscillations. *Phys. Rev. Lett.* **32**, 1420–1423.
KOPNIN, S.I., SHOKHRIN, D.V. & POPEL, S.I. 2022 Dust acoustic solitons in Saturn's dust-filled magnetosphere. *Plasma Phys. Rep.* **48**, 141–146.

LUNDIN, R., ZAKHAROV, A., PELLINEN, R., BORG, H., HULTQVIST, B., PISSARENKO, N., DUBININ, E.M., BARABASH, S.W., LIEDE, I. & KOSKINEN, H. 1989 First measurements of the ionospheric plasma escape from Mars. *Nature* **341**, 609–612.

MAITY, C. 2014 Phase-mixing of Langmuir oscillations in cold electron-positron-ion plasmas. *Phys. Plasmas* **21**, 072317.

MAITY, C., CHAKRABARTI, N. & SENGUPTA, S. 2012 Breaking of upper hybrid oscillations in the presence of an inhomogeneous magnetic field. *Phys. Rev. E* **86**, 016408.

MAITY, C. & KARMAKAR, M. 2023 Wave breaking amplitudes of Langmuir modes in electron-positron-ion-dusty plasmas. *Phys. Scr.* **98**, 085601.

MAITY, C. & PRAMANIK, S. 2020 Effects of finite ion inertia on phase-mixing of Langmuir oscillations in cold electron-positron-ion plasmas. *Phys. Lett. A* **384**, 126856.

MAITY, C., SARKAR, A., SHUKLA, P.K. & CHAKRABARTI, N. 2013 Wave-breaking phenomena in a relativistic magnetized plasma. *Phys. Rev. Lett.* **110**, 215002.

MALKA, V. 2012 Laser plasma accelerators. *Phys. Plasmas* **19**, 055501.

MAMUN, A.A., FERDOUSI, M. & SULTANA, S. 2015 Dust-acoustic solitary waves in a magnetized opposite polarity dust-plasma medium. *Phys. Scr.* **90**, 088011.

MAMUN, A.A. & MANNAN, A. 2011 Nonplanar double layers in plasmas with opposite polarity dust. *JETP Lett.* **94**, 356–361.

MAMUN, A.A. & SHUKLA, P.K. 2011 Discoveries of waves in dusty plasmas. *J. Plasma Phys.* **77**, 437–455.

MENDIS, D.A. & ROSENBERG, M. 1994 Cosmic dusty plasmas. *Annu. Rev. Astron. Astrophys.* **32**, 419–463.

MERLINO, R.L. 2009 Dust-acoustic waves driven by an ion-dust streaming instability in laboratory discharge dusty plasma experiments. *Phys. Plasmas* **16**, 124501.

MERLINO, R.L. 2014 25 years of dust acoustic waves. *J. Plasma Phys.* **80**, 773–786.

MERLINO, R.L., BARKAN, A., THOMPSON, C. & D'ANGELO, N. 1998 Laboratory studies of waves and instabilities in dusty plasmas. *Phys. Plasmas* **5**, 1607–1614.

MERLINO, R.L., HEINRICH, J.R., HYUN, S.-H. & MEYER, J.K. 2012*a* Nonlinear dust acoustic waves and shocks. *Phys. Plasmas* **19**, 057301.

MERLINO, R.L., HEINRICH, J.R., KIM, S.-H. & MEYER, J.K. 2012*b* Dusty plasmas: experiments on nonlinear dust acoustic waves, shocks and structures. *Plasma Phys. Control. Fusion* **54**, 124014.

MEYER-VERNET, N. 1982 Flip-flop of electric potential of dust grains in space. *Astron. Astrophys.* **105**, 98–106.

MODENA, A. *et al.* 1995 Electron acceleration from the breaking of relativistic plasma waves. *Nature* **377**, 606–608.

MOROOKA, M.W., WAHLUND, J., ERIKSSON, A.I., FARRELL, W.M., GURNETT, D.A., KURTH, W.S., PERSOON, A.M., SHAFIQ, M., ANDRÉ, M. & HOLMBERG, M.K.G. 2011 Dusty plasma in the vicinity of Enceladus. *J. Geophys. Res.* **116**, 2011JA017038.

NAKAMURA, Y. & BAILUNG, H. 1999 A dusty double plasma device. *Rev. Sci. Instrum.* **70**, 2345–2348.

NAYFEH, A.H. 2000 *Perturbation Methods*. 1st edn. Wiley-Interscience.

PETERSEN, A., ASNAZ, O.H., TADSEN, B. & GREINER, F. 2022 Decoupling of dust cloud and embedding plasma for high electron depletion in nanodusty plasmas. *Commun. Phys.* **5**, 308.

PRAMANIK, S., BISWAS, A. & MAITY, C. 2024 Ion motion can cause nonlinear electron acoustic waves in plasmas to phase-mix: a theoretical study. *Phys. Plasmas* **31**, 092110.

PRAMANIK, S. & MAITY, C. 2017 Effects of magnetic field on phase-mixing of electrostatic oscillations in cold electron-positron-ion plasmas. *Phys. Plasmas* **24**, 084504.

PRAMANIK, S. & MAITY, C. 2018 Langmuir wave phase-mixing in warm electron-positron-dusty plasmas. *Phys. Lett. A* **382**, 1020–1023.

PRAMANIK, S. & MAITY, C. 2021 On Langmuir oscillations breaking driven by ion motion and relativistic effects. *Phys. Scr.* **96**, 035603.

PRAMANIK, S., MAITY, C. & CHAKRABARTI, N. 2015 Phase-mixing of ion plasma modes in pair-ion plasmas. *Phys. Plasmas* **22**, 052303.

RAO, N., SHUKLA, P. & YU, M. 1990 Dust-acoustic waves in dusty plasmas. *Planet. Space Sci.* **38**, 543–546.

RAO, N.N. 1998 Linear and nonlinear dust-acoustic waves in non-ideal dusty plasmas. *J. Plasma Phys.* **59**, 561–574.

ROSENBERG, M. 2002 A note on ion–dust streaming instability in a collisional dusty plasma. *J. Plasma Phys.* **67**, 235–242.

ROSENBERG, M. & KALMAN, G. 1997 Dust acoustic waves in strongly coupled dusty plasmas. *Phys. Rev. E* **56**, 7166–7173.

ROSENBERG, M. & MENDIS, D.A. 1995 UV-induced Coulomb crystallization in a dusty gas. *IEEE Trans. Plasma Sci.* **23**, 177–179.

ROSENBERG, M., MENDIS, D.A. & SHEEHAN, D.P. 1999 Positively charged dust crystals induced by radiative heating. *IEEE Trans. Plasma Sci.* **27**, 239–242.

SAHAI, A.A. 2017 Excitation of a nonlinear plasma ion wake by intense energy sources with applications to the crunch-in regime. *Phys. Rev. Accelerators Beams* **20**, 081004.

SAKANAKA, P.H. & SHUKLA, P.K. 2000 Large amplitude solitons and double layers in multicomponent dusty plasmas. *Phys. Scr.* **T84**, 181.

SEN GUPTA, S. & KAW, P.K. 1999 Phase mixing of nonlinear plasma oscillations in an arbitrary mass ratio cold plasma. *Phys. Rev. Lett.* **82**, 1867–1870.

SENGUPTA, S., SAXENA, V., KAW, P.K., SEN, A. & DAS, A. 2009 Phase mixing of relativistically intense waves in a cold homogeneous plasma. *Phys. Rev. E* **79**, 026404.

SHIKHA, R.K., CHOWDHURY, N.A., MANNAN, A. & MAMUN, A.A. 2019 Dust-acoustic rogue waves in an electron depleted plasma. *Eur. Phys. J. D* **73**, 177.

SHUKLA, P. & L., I. 2010 Dust acoustic wave breaking in a strongly coupled dusty plasma. *Phys. Lett. A* **374**, 1165–1166.

SHUKLA, P.K. 2000 Dust acoustic wave in a thermal dusty plasma. *Phys. Rev. E* **61**, 7249–7251.

SHUKLA, P.K. 2001 A survey of dusty plasma physics. *Phys. Plasmas* **8**, 1791–1803.

SHUKLA, P.K. 2003 Nonlinear waves and structures in dusty plasmas. *Phys. Plasmas* **10**, 1619–1627.

SHUKLA, P.K. & MAMUN, A.A. 2010 *Introduction to Dusty Plasma Physics*. Taylor and Francis.

SHUKLA, P.K. & ROSENBERG, M. 2006 Streaming instability in opposite polarity dust plasmas. *Phys. Scr.* **73**, 196–197.

SINGH, S.V. 2002 Dust-acoustic waves with a non-thermal ion velocity distribution. In *AIP Conference Proceedings*, vol. 649, pp. 442–445. AIP.

TADSEN, B., GREINER, F., GROTH, S. & PIEL, A. 2015 Self-excited dust-acoustic waves in an electron-depleted nanodusty plasma. *Phys. Plasmas* **22**, 113701.

TRIBECHE, M. & MERRICHE, A. 2011 Nonextensive dust-acoustic solitary waves. *Phys. Plasmas* **18**, 034502.

TRUKHACHEV, F.M., VASILIEV, M.M., PETROV, O.F. & VASILIEVA, E.V. 2019 Dust-acoustic soliton breaking and the associated acceleration of charged particles. *Phys. Rev. E* **100**, 063202.

VERHEEST, F. 2000 Waves in dusty space plasmas. In *Astrophysics and Space Science Library*, vol. 245, Springer Netherlands.

VERHEEST, F. 2009 Nonlinear acoustic waves in nonthermal plasmas with negative and positive dust. *Phys. Plasmas* **16**, 013704.

VERHEEST, F., HELLBERG, M.A. & KOURAKIS, I. 2008 Acoustic solitary waves in dusty and/or multi-ion plasmas with cold, adiabatic, and hot constituents. *Phys. Plasmas* **15**, 112309.

VERHEEST, F., SHUKLA, P.K., RAO, N.N. & MEURIS, P. 1997 Dust-acoustic waves in self-gravitating dusty plasmas with fluctuating dust charges. *J. Plasma Phys.* **58**, 163–170.

VERMA, P.S. 2011 Nonlinear oscillations and waves in an arbitrary mass ratio cold plasma. *Phys. Plasmas* **18**, 122111.

WAHLUND, J.-E. *et al.* 2009 Detection of dusty plasma near the E-ring of Saturn. *Planet. Space Sci.* **57**, 1795–1806.

WATSON, G.N. 2006 *A Treatise on the Theory of Bessel Functions*. 2nd edn. Cambridge University Press.

WHIPPLE, E.C., NORTHROP, T.G. & MENDIS, D.A. 1985 The electrostatics of a dusty plasma. *J. Geophys. Res.* **90**, 7405–7413.

XU, H., SHENG, Z.-M. & ZHANG, J. 2006 Phase mixing due to ion motion and relativistic effects in nonlinear plasma oscillations. *Phys. Scr.* **74**, 673–677.

YU, L.-L., ZHAO, Y., QIAN, L.-J., CHEN, M., WENG, S.-M., SHENG, Z.-M., JAROSZYNSKI, D.A., MORI, W.B. & ZHANG, J. 2016 Plasma optical modulators for intense lasers. *Nat. Commun.* **7**, 11893.

ZHAO, H., CASTLE, G.S.P., INCULET, I.I. & BAILEY, A.G. 2003 Bipolar charging of poly-disperse polymer powders in fluidized beds. *IEEE Trans. Ind. Applics.* **39**, 612–618.

ZHAO, H., CASTLE, G.S.P. & INCULET, I.I. 2002 The measurement of bipolar charge in polydisperse powders using a vertical array of Faraday pail sensors. *J. Electrostat.* **55**, 261–278.

https://doi.org/10.1017/S0022377825100585 Published online by Cambridge University Press